Acta Crystallographica Section F
Structural Biology and Crystallization Communications
ISSN 1744-3091

High-resolution structure of a new crystal form of BamA POTRA4–5 from *Escherichia coli*

Heng Zhang,[a,b] Zeng-Qiang Gao,[b] Hai-Feng Hou,[b] Jian-Hua Xu,[b] Lan-Fen Li,[a] Xiao-Dong Su[a]* and Yu-Hui Dong[b]*

[a]National Laboratory of Protein Engineering and Plant Genetic Engineering, College of Life Science, Peking University, Beijing 100871, People's Republic of China, and [b]Beijing Synchrotron Radiation Facility, Institute of High Energy Physics, Chinese Academy of Sciences, Beijing 100049, People's Republic of China

Correspondence e-mail: xdsu@pku.edu.cn, dongyh@ihep.ac.cn

Received 18 January 2011
Accepted 15 April 2011

PDB Reference: BamA POTRA4–5, 3q6b.

In *Escherichia coli*, the BAM complex is employed to mediate correct folding of the outer membrane (OM) proteins into β-barrels and their insertion into the OM. BamA, which is an essential component of the complex, consists of a C-terminal transmembrane region and five N-terminal polypeptide transport-associated (POTRA) domains. Although deletion studies have shown that each of the POTRA domains plays an important role in the process of BAM complex formation, only POTRA5 is essential for cell viability. Here, the crystal structure of POTRA4–5 has been determined to 1.50 Å resolution with an R factor of 14.7% and an $R_{\rm free}$ of 18.9%.

1. Introduction

The periplasmic space of Gram-negative bacteria is enveloped by two membranes. One is the plasma membrane (inner membrane; IM) and the other is the outer membrane (OM). The distinguishing characteristic of the OM is its composition. Lipopolysaccharides (LPS) are found in the outer leaflet of the OM. In contrast, phospholipids are located in the inner leaflet of the OM. The IM consists of a symmetrical phospholipid bilayer inlaid with α-helical membrane proteins, but the outer membrane proteins (OMPs) that reside on the OM are β-barrels (Schulz, 2003; Wimley, 2003).

Proteins delivered to the OM are synthesized in the cell plasma as β-barrel protein precursors. Subsequently, a translocase known as the SecYEG translocon mediates translocation of the nascent OMPs across the IM (Driessen & Nouwen, 2008; Veenendaal *et al.*, 2004). After the SecYEG machinery has released the preproteins into the periplasm, their N-terminal signal sequences are cleaved by signal peptidase.

The chaperones SurA, Skp and DegP are involved in transporting β-barrel protein precursors through periplasmic space to the outer membrane (Mogensen & Otzen, 2005). One major function of chaperones is to prevent unfolded OMPs from aggregating into misfolded structure. Some chaperones, such as DegP, also perform another function: they act as a protease to degrade excess precursors (Sklar *et al.*, 2007; Knowles *et al.*, 2009).

In *Escherichia coli* the β-barrel assembly machine (BAM) catalyzes the insertion of processed OMPs into the OM. BAM, a multi-protein complex, is composed of four lipoproteins, BamB, BamC, BamD and BamE (formerly YfgL, NlpB, YfiO and SmpA, respectively), and an integral membrane protein known as BamA (formerly YaeT) (Wu *et al.*, 2005; Walther *et al.*, 2009). Previous mutagenesis analysis has revealed that only BamA and BamD are essential for cell survival and OMP biogenesis (Voulhoux *et al.*, 2003; Wu *et al.*, 2005). Strains that lack BamB, BamC and BamE are still viable, whereas null mutations in these genes result in OMPs with folding defects and sensitivity to antibiotics. Based on knockout experiments, BamB appears to affect the activity of OMP assembly independent of the SurA pathway (Sklar *et al.*, 2007; Vuong *et al.*, 2008). BamA binds

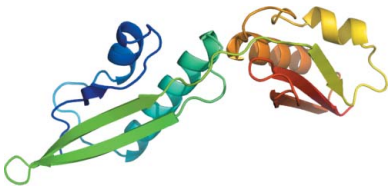

BamB through a β-augmentation and also makes a direct interaction with BamD. BamE is required to stabilize the interaction between BamA and BamD. However, the C-terminus of BamD is involved in the binding of BamC to BamA (Kim *et al.*, 2007; Vuong *et al.*, 2008; Knowles *et al.*, 2009).

BamA, also known as Omp85, is highly conserved in Gram-negative bacteria. Homologous proteins also exist in chloroplasts (Sam50) and mitochondria (Toc75) in eukaryotes (Wimley, 2003). BamA consists of five soluble POTRA (polypeptide transport-associated) domains and a membrane-embedded β-barrel domain. The five POTRA domains are nearly the same size, with a molecular weight ranging between 7 and 10 kDa.

The role of POTRA domains in OMP biogenesis is still not clear, but pull-down studies have shown that the POTRA domains seem to provide a scaffold for other components of the BAM complex and bind unfolded β-barrel precursors. POTRA domains can also act as a chaperone to stimulate OMP folding. Deletion of POTRA1 and POTRA2 leads to mild OMP biogenesis defects but no fatal effects, while POTRA3–5 are essential for cell survival. Conversely, only POTRA5 is required, and removal of POTRA5 results in cell death, in *Neisseria meningitides* (Bos *et al.*, 2007; Kim *et al.*, 2007). Two POTRA1–4 crystal structures have been reported (Kim *et al.*, 2007; Gatzeva-Topalova *et al.*, 2008). These structures exhibit conformational flexibility between the POTRA2 and POTRA3 domains, suggesting the presence of a kink region between them. In addition, the structure of POTRA 1–2 has been solved by NMR (Knowles *et al.*, 2008).

Compared with the recently reported 2.70 Å resolution crystal structure of POTRA 4–5 (Gatzeva-Topalova *et al.*, 2010), the crystal structure presented here has a higher resolution (1.50 Å) and belongs to a different space group.

2. Materials and methods

2.1. Cloning, expression and purification

To construct a plasmid carrying the N-terminal domain of BamA (residues 266–420), the following primers were designed: 5′-CGC-GGATCCGCTGAAATCCAGCAAATT-3′ and 5′-CCGCTCGAG-TTACTCTTTTACCTTGTAGACGAC-3′. The gene was amplified from genomic *Escherichia coli* DNA by polymerase chain reaction (PCR). The PCR product digested with *Bam*HI and *Xho*I overnight at 310 K was introduced into pET28at-plus, which is a modified pET28a(+) plasmid (Novagen). The recombinant plasmid with an N-terminal His_6 tag (MGSSHHHHHHSSGENLYFEGSHMASMT-GGQQMGR) was transformed into *E. coli* strain BL21 (DE3) for expression. The transformed cells were grown in 20 ml Luria–Bertani (LB) medium at 310 K overnight and then transferred into 1 l fresh LB medium containing 50 µg ml^{-1} kanamycin; growth was continued at 310 K until the OD_{600} reached 0.6. Isopropyl β-D-1-thiogalacto-pyranoside was then added to the culture to a final concentration of 0.5 m*M* to induce recombinant protein expression at 303 K for a further 6 h. After incubation, the cells were harvested by centrifugation (8000 rev min^{-1}, 15 min, 277 K) and resuspended in 25 ml buffer *A* (20 m*M* Tris–HCl pH 7.5, 5% glycerol, 500 m*M* NaCl).

The resuspended cells were disrupted by sonication on ice and then centrifuged twice (20 000 rev min^{-1}, 30 min, 277 K) to remove debris. The supernatant was loaded onto 2 ml Chelating Sepharose Fast Flow resin (GE Healthcare) pre-equilibrated with buffer *A*. The resin was washed with 20 ml buffer *A* and the target protein was eluted with an imidazole gradient (20, 50, 100 and 500 m*M*) in buffer *A*. After SDS–PAGE analysis, 5 ml eluate (20 m*M* Tris–HCl pH 7.5, 5% glycerol, 500 m*M* NaCl, 500 m*M* imidazole) was pooled and concentrated to 1 ml by ultrafiltration using a Millipore centrifugal device (Amicon Ultra, 3 kDa cutoff). The protein was applied onto a Superdex 200 column (120 ml, GE Healthcare) equilibrated with buffer *C* (20 m*M* Tris–HCl pH 7.5, 5% glycerol, 200 m*M* NaCl).

Table 1
Data-collection and structure-refinement statistics.

Values in parentheses are for the highest resolution shell.

	3q6b	3og5
Data collection		
Wavelength (Å)	0.9791	0.9798
Space group	*C*2	$P3_221$
Unit-cell parameters (Å, °)	a = 137.53, b = 39.01, c = 32.56, β = 101.00	$a = b$ = 118.49, c = 69.99
Resolution (Å)	1.50 (1.55–1.50)	2.70 (2.80–2.70)
No. of unique reflections	26711 (2260)	
Completeness (%)	97.5 (83.1)	96.8 (97.3)
Multiplicity	4.5 (2.6)	1.5 (1.4)
Mean $I/\sigma(I)$	32.8 (2.83)	8.4 (2.6)
Molecules in asymmetric unit	1	2
Matthews coefficient (Å^3 Da^{-1})	2.46	3.75
Solvent content (%)	49.03	67.16
R_{merge}† (%)	7.4 (33.6)	8.4 (24.2)
Structure refinement		
Resolution range (Å)	25.8–1.50	38.79–2.69
R_{work}/R_{free} (%)	14.7/18.9	21.2/26.0
No. of residues/protein atoms	155/1281	
No. of water atoms	141	
Average B factors (Å^2)		
Main chain	22.7	25.6
Side chains	29.4	32.7
Overall	26.1	29.1
Waters	37.6	31.4
Ramachandran plot (%)		
Most favoured	98.7	89.4
Allowed	1.3	10.6
Disallowed	0.0	0.0
R.m.s. deviations		
Bond lengths (Å)	0.005	0.009
Bond angles (°)	0.938	1.200

† $R_{merge} = \sum_{hkl}\sum_i |I_i(hkl) - \langle I(hkl)\rangle| / \sum_{hkl}\sum_i I_i(hkl)$.

2.2. Crystallization and data collection

After gel filtration, fractions containing target protein were pooled and concentrated to 12 mg ml^{-1} as quantified using a Bio-Rad protein-assay kit. Crystallization trials were performed by the sitting-drop vapour-diffusion method at 293 K. Several commercial kits such as Crystal Screen, Crystal Screen 2 and Natrix (Hampton Research) were used as initial screening conditions. 1 µl protein solution was mixed with 1 µl reservoir solution and equilibrated against 130 µl reservoir solution in a 48-well plate (XtalQuest Inc., Beijing, People's Republic of China). Needle-shaped and flower-shaped crystals appeared in several conditions after 10 d, but only the needle-shaped crystals diffracted well. Finally, crystals suitable for X-ray diffraction experiments were obtained using the following conditions: 0.2 *M* sodium acetate trihydrate, 0.1 *M* sodium cacodylate trihydrate pH 6.5, 30%(*w*/*v*) polyethylene glycol (PEG) 8000. The crystal belonged to space group *C*2, with unit-cell parameters a = 137.53, b = 39.01, c = 32.56 Å, β = 101.00°.

The crystal was soaked in cryoprotectant consisting of mother liquor containing 15%(*v*/*v*) glycerol for a few seconds and flash-cooled in liquid nitrogen at 100 K. Diffraction data were collected on the BL17U-MX beamline at SSRF (Shanghai Synchrotron Radiation Facility, Shanghai, People's Republic of China) using a MAR 225 CCD detector at a wavelength of 0.9791 Å. The total oscillation was 360° with 1° per image and the exposure time was 1 s per image. The sample-to-detector distance was set to 120 mm. The data were

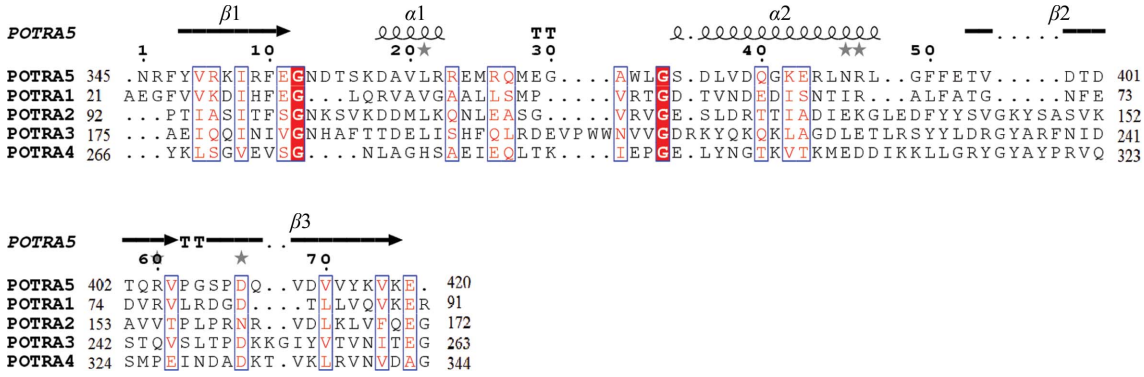

Figure 1
Multiple sequence alignment of the five POTRA domains using *ClustalW* (Thompson *et al.*, 1994). The figure was generated with *ESPript* (Gouet *et al.*, 1999). Conserved residues are shown on a red background and residues with high similarly are coloured red.

processed with *HKL*-2000 (Otwinowski & Minor, 1997) and the statistical results are listed in Table 1.

2.3. Structure determination and refinement

The initial phases were calculated using *Phaser* (McCoy, 2007) with the low-resolution structure of POTRA4–5 chain *A* (PDB entry 3og5; Gatzeva-Topalova *et al.*, 2010) as the search model. The phases from *Phaser* and the structure factors from *HKL*-2000 could be combined in *ARP*/*wARP* (Perrakis *et al.*, 1999) directly owing to the high data quality (Table 1) and 150 of 155 residues were traced. Some bias was reduced manually in *Coot* (Emsley & Cowtan, 2004). The program *phenix.refine* (Afonine *et al.*, 2005) was used to refine the structure and to append water molecules.

PROCHECK (Laskowski *et al.*, 1993) was used to validate the structure. The final refinement statistics are listed in Table 1.

3. Results and discussion

The 1.5 Å resolution crystal structure of BamA POTRA4–5 from *E. coli* (PDB entry 3q6b) was solved by molecular replacement using PDB entry 3og5 as the search target. The crystal belonged to space group *C*2 and there was one protein molecule in the asymmetric unit, with a Matthews coefficient of 2.46 Å^3 Da^{-1}, corresponding to a solvent content of almost 50% (Matthews, 1968). In the structure reported by Gatzeva-Topalova *et al.* (2010), however, the crystal belonged to space group $P3_221$ and there were two molecules in the asymmetric unit.

BamA contains five POTRA domains; the first four POTRA domains possess a conserved fold consisting of a pair of antiparallel helices covered by a mixed three-stranded β-sheet, despite their low sequence identity (Fig. 1). Most of these residues are found in α-helices or β-strands. The POTRA5 domain also shares this architecture (Kim *et al.*, 2007; Gatzeva-Topalova *et al.*, 2008, 2010).

The final structure contains 155 residues (Tyr266–Glu420) and 141 water molecules. The R and $R_{\rm free}$ factors were 14.7% and 18.9%, respectively (Table 1). The overall configuration of the POTRA4–5 domains (Fig. 2*a*) is similar to the previously published model (PDB entry 3og5). There are two molecules in the asymmetric unit in the 3og5 structure (chains *A* and *B*): chain *A* contains residues Asp264–Arg421 and has an average *B* factor of 29.1 Å^2, while chain *B* contains 21 fewer residues (Gly270–Val271, Ile290–Gly293, Pro326–Val335 and Asp358–Asp362) because of poor density and has an average *B* factor of 60.0 Å^2. Therefore, chain *A* of 3og5 (referred to in this paper as 3og5-*A*) was chosen for comparison with the present structure. According to the refinement statistics, the structure reported here is more accurate (Table 1). First of all, our structure has a higher resolution: the diffraction data quality and final electron density both indicate that the high resolution is reliable. Secondly, the R and $R_{\rm free}$ factors are 6.5% and 7.1% lower than those of 3og5, respectively.

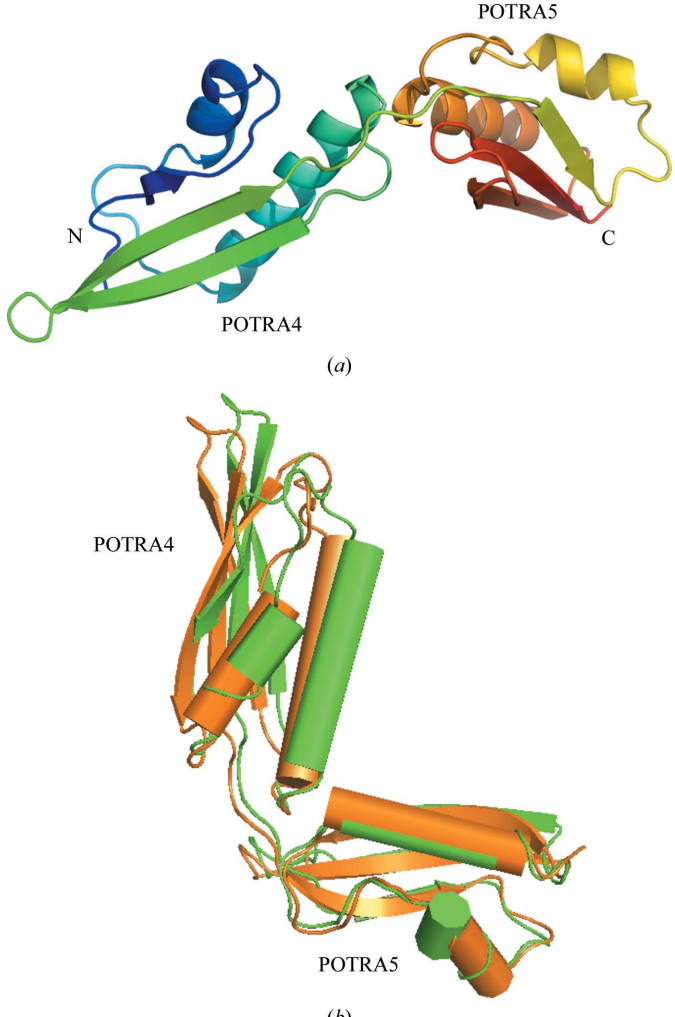

Figure 2
(*a*) Overall structure of POTRA4–5 in cartoon representation (N-terminus, blue; C-terminus, red). (*b*) Superimposition of the present structure (green) and that of Gatzeva-Topalova and coworkers (orange; Gatzeva-Topalova *et al.*, 2010).

Thirdly, the average B factors for the main chain, side chains and water molecules are all lower than those of 3og5, which means that the overall structure is more reliable than 3og5, although two loops are more flexible (as discussed in the following paragraph). Lastly, the percentage of residues in the most favoured regions of the Ramachandran plot in our structure is 9.3% higher than that of 3og5, which means that the conformations of the φ–ψ dihedral angles in the present structure are more favourable than that of 3og5.

The crystal packings in the two structures are different (Table 2; Figs. 3*a* and 3*b*). 15 residues in chain *A* and three residues in chain *B* are involved in crystal contacts between symmetry-related molecules in 3og5. Ten of these residues (Gln286, Lys303, Arg314, Lys351, Thr359, Lys361, Arg367, Glu373, Gly374 and Asp380) are also involved in crystal contacts in 3q6b. However, the residues which form hydrogen bonds to these ten residues differ between the two structures. In 3og5, Thr359 and Lys361 are involved in two hydrogen bonds to Ile*290 from a symmetry-related molecule ($-y+1, x-y+1, z+2/3$) (Thr359 O···Ile*290 N, Lys361 N···Ile*290 O) and the remaining eight residues are involved in contacts between two molecules related by the symmetry operation ($-y+1, x-y+1, z-1/3$) (Gln286 NE2···Arg**370 O, Lys303 NZ···Gly**374 O, Arg314 NH1 ···Glu**373 OE1, Gly279 O···Arg367 NH1, Asp380 OD1··· Arg353 NH1, Glu387 OE2···Lys351 NZ). In 3q6b these ten residues are involved in hydrogen bonds to several molecules related by four symmetry operations. Thr359, Lys361, Arg367, Glu373 and Gly374 are involved in hydrogen bonds to Gln′286, Gln′286, Asp′307, Gln′384 and Arg′391, respectively, from the symmetry-related molecule ($-x+1/2, y-1/2, -z$) (Thr359 O···Gln′286 NE2, Lys361 N···Gln′286 OE1, Arg367 NH1···Asp307 OD2, Glu373 OE1 ···Gln384 NE2, Gly374 O···Arg391 NH1), Lys351 forms a hydrogen bond to Glu′′396 from the symmetry-related molecule ($-x+1/2, y-1/2, -z-1$) (Lys351 NZ···Glu′′396 OE2), Arg$^{\#}$314 and Asp$^{\#}$380 from the symmetry-related molecule ($x, y, z-1$) are hydrogen bonded to Lys419 and Glu396 (Lys419 NZ···Arg$^{\#}$314 O, Lys419 NZ ···Asp$^{\#}$380 OD2, Glu396 OE1···Arg$^{\#}$314 NH2) and Lys$^{\#\#}$303 from the symmetry-related molecule ($x, y-1, z$) forms a hydrogen bond to Ser408 (Ser408 OG···Lys$^{\#\#}$303 NZ).

The overall structure of POTRA4–5 is shaped like a capital L when seen from the side. The POTRA4 and POTRA5 domains are joined by a short linker (Gly344-Asn345-Arg346) and oriented at an angle

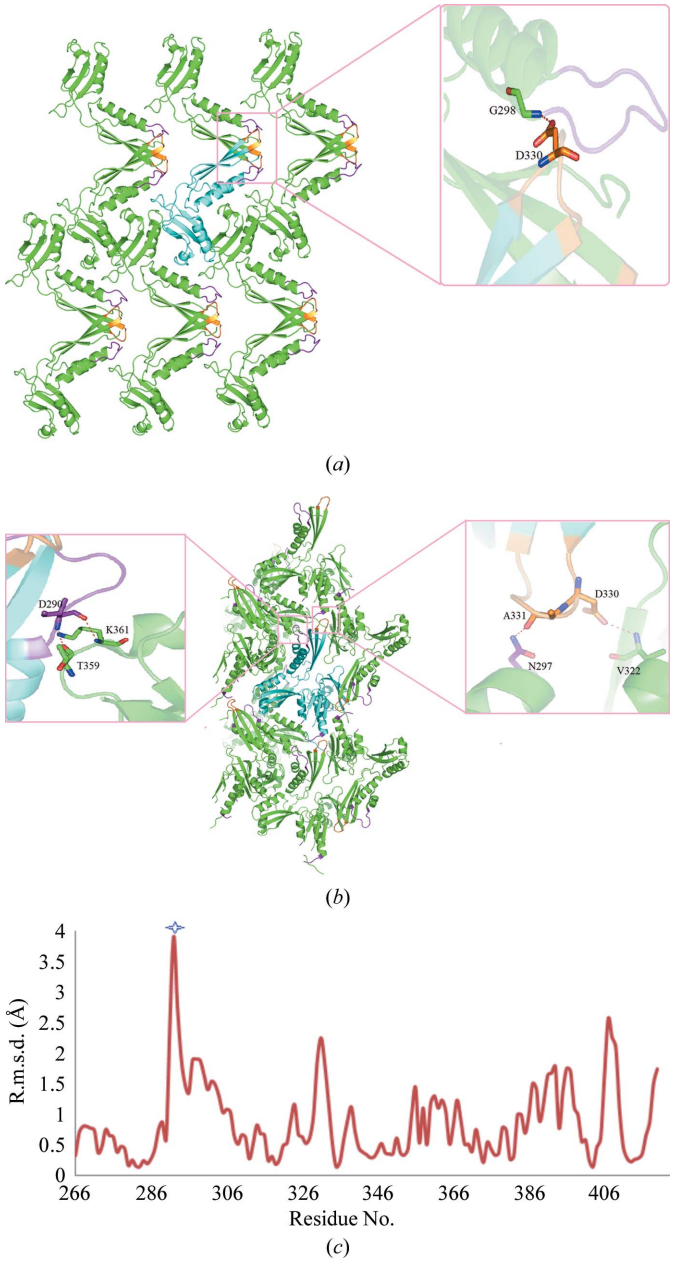

Figure 3
(*a*, *b*) Crystal packing of POTRA4–5 in space groups *C*2 (this study) and $P3_221$ (PDB entry 3og5; Gatzeva-Topalova *et al.*, 2010), respectively. Symmetry-related molecules that make direct hydrogen-bonded contacts with the central molecule (cyan) are shown in green, with loop 2 in POTRA4 in magenta and loop 4 in POTRA4 in orange. The hydrogen bonds between the molecules are shown in the insets. (*c*) R.m.s.d. plot of the main-chain atoms of the POTRA4–5 structure (PDB entry 3q6b) and chain *A* of PDB entry 3og5. The r.m.s.d. was calculated using the program *LSQKAB* (Winn *et al.*, 2011). Residue Pro292 is indicated by a star.

Table 2
Protein–protein contacts between the symmetry-related molecules in our structure (3q6b) and that previously reported (3og5).

Atom *X*	Atom *Y*	Distance (Å)	Symmetry operation
3og5			
Gln*A*286 NE2	Arg*A*370 O	3.46	$-y+1, x-y+1, z-1/3$
Arg*A*314 NH1	Glu*A*373 OE1	2.66	
Lys*A*303 NZ	Gly*A*374 O	2.81	
Gly*A*279 O	Arg*A*367 NH1	3.00	
Asp*A*380 OD1	Arg*A*353 NH1	2.40	
Glu*A*387 OE2	Lys*A*351 NZ	3.11	
Glu*A*387 OE2	Arg*A*353 NH2	2.43	
Arg*B*321 NH1	Tyr*A*266 OH	3.33	$x-y+1, -y+2, -z+1/3$
Val*B*322 N	Asp*A*330 OD1	2.92	
Arg*B*404 N	Glu*A*327 OE2	2.67	
Arg*B*404 NE	Gln*A*323 NE2	2.77	
Thr*B*302 OG1	Thr*B*302 OG1	2.68	$x-y+1, -y+2, -z+4/3$
Asn*B*340 ND2	Asp*B*264 OD1	2.70	
Asp*B*264 OD1	Asn*B*340 ND2	2.70	
Lys*A*361 N	Ile*A*290 O	2.87	$-y+1, x-y+1, z+2/3$
Thr*A*359 O	Ile*A*290 N	2.76	
Ala*A*331 O	Asn*B*297 ND2	2.66	$x, y, z-1$
Tyr*A*266 OH	Gln*B*265 OE1	3.48	
3q6b			
Ala363 N	Glu283 OE2	2.87	$-x+1/2, y-1/2, -z$
Lys361 N	Gln286 OE1	2.81	
Arg367 NH1	Leu287 O	3.05	
Arg367 NH1	Asp307 OD2	2.90	
Thr359 O	Gln286 NE2	2.87	
Glu373 OE1	Gln384 NE2	3.12	
Gly374 O	Arg391 NH1	3.33	
Gly298 N	Asp330 OD1	2.73	$-x, y, -z$
Asp330 OD1	Gly298 N	2.73	
Lys351 NZ	Glu396 OE2	2.57	$-x+1/2, y-1/2, -z-1$
Asp358 OD1	Asn390 ND2	3.37	
Thr397 OG1	Tyr315 OH	3.16	$x, y, z-1$
Lys419 NZ	Arg314 O	3.17	
Lys419 NZ	Asp380 OD2	2.84	
Glu396 OE1	Arg314 NH2	2.74	
Ser408 OG	Lys303 NZ	3.07	$x, y-1, z$

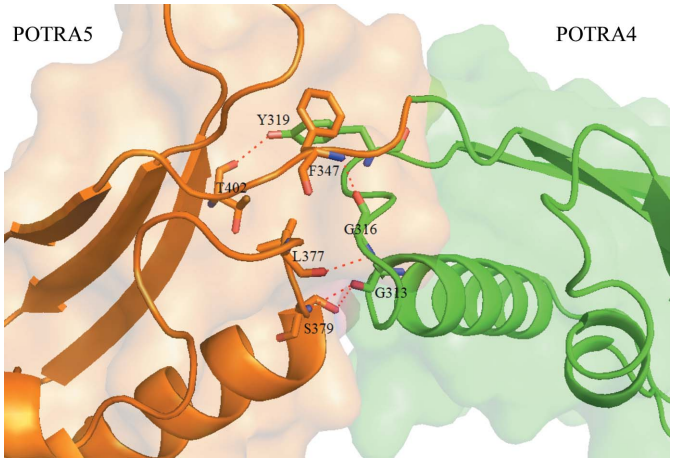

Figure 4
Interface between POTRA4 (green) and POTRA5 (orange). Residues are shown as sticks and hydrogen bonds are indicated by red dashed lines. This representation was generated with *PyMOL* (DeLano, 2002).

of about 90°. The relative orientation of POTRA4 and POTRA5 is a little different in the two structures. In the present structure the POTRA4 domain is closer to the POTRA5 domain (Fig. 2*b*). However, the interface interactions are identical (Fig. 4). Hydrogen bonds between the main-chain atoms of Gly313 and Ser379, Gly316 and Phe347, and Gly316 and Leu377, as well as between the hydroxyl group of Tyr319 and the carbonyl group of Thr402, contribute to the stability of the whole structure. One exception is the interaction of Arg314: the salt bridge between its guanidinium group and Asp383 and the hydrogen bond to Ser379 are missing in the present structure. Considering that these interactions are also missing in chain *B* of 3og5, it may be concluded that the interactions of Arg314 are not important to the interface.

On the whole, the present structure is very similar to 3og5, but there are some subtle differences. *LSQKAB* (Winn *et al.*, 2011) was used to compare the main-chain atoms of our structure with those of 3og5-*A*. The average root-mean-square deviation (r.m.s.d.) between the present structure and 3og5-*A* is 1.062 Å over 155 C^{α} atoms and the maximum deviation is 3.923 Å for Pro292. Apart from residue Pro292, significant differences (>2 Å) are seen in various residues, including residues Glu291, Gly293, Ala331, Gly407, Ser408 and Pro409 (Fig. 3*c*). Those residues all lie in loop regions such as loop 2 (Lys289–Asn297) and loop 4 (Asn329–Thr334) of POTRA4 (Fig. 3*a*). The overall *B* factors of these regions are 36.86 and 43.65 $Å^2$ in 3og5-*A* but are 44.65 and 50.83 $Å^2$ in 3q6b, suggesting that these regions are more flexible in our structure compared with the other regions. Through analysis of contacts in the two crystals, a relationship between loop flexibility and crystal packing can be built. The loop 2s of two neighbouring molecules in the 3og5 crystal lattice interact with each other *via* two hydrogen bonds (Fig. 3*b*). In the case of loop 4 in the 3og5 crystal, an interaction involving residue Asp330 with Val322 of a symmetry-related molecule is observed. An additional contact is observed between Ala330 and Asn297 of another neighbouring molecule (Fig. 3*b*). In contrast, in our crystal only Asp330 in loop 4 forms a hydrogen bond to Gly298 from a symmetry-related molecule (Fig. 3*a*). The increased contacts in the 3og5 crystal may result in a more stable packing arrangement. We are currently assessing whether these loops would be more flexible in 3og5 if these contacts were lost, as observed in our crystal. It will be worth making further studies to determine whether these regions make interactions with other components of the BAM complex.

4. Conclusions

This work reports a crystal structure of POTRA4–5 that differs from that previously reported (Gatzeva-Topalova *et al.*, 2010): it was refined to 1.50 Å resolution and belonged to space group *C*2. As a consequence of its high resolution, it is similar to but more accurate than the previous structure.

We thank the staff of the SSRF beamline and Drs Jiahai Zhou and Weixue Huang of the Shanghai Institute of Organic Chemistry, Chinese Academy of Sciences for assistance in data collection; we also would like to thank Dr Xiang Liu of the College of Life Science, Peking University for helpful discussion and comments.

References

Afonine, P. V., Grosse-Kunstleve, R. W. & Adams, P. D. (2005). *CCP4 Newsl. Protein Crystallogr.* **42**, contribution 8.
Bos, M. P., Robert, V. & Tommassen, J. (2007). *Annu. Rev. Microbiol.* **61**, 191–214.
DeLano, W. L. (2002). *PyMOL*. http://www.pymol.org.
Driessen, A. J. & Nouwen, N. (2008). *Annu. Rev. Biochem.* **77**, 643–667.
Emsley, P. & Cowtan, K. (2004). *Acta Cryst.* D**60**, 2126–2132.
Gatzeva-Topalova, P. Z., Walton, T. A. & Sousa, M. C. (2008). *Structure*, **16**, 1873–1881.
Gatzeva-Topalova, P. Z., Warner, L. R., Pardi, A. & Sousa, M. C. (2010). *Structure*, **18**, 1492–1501.
Gouet, P., Courcelle, E., Stuart, D. I. & Métoz, F. (1999). *Bioinformatics*, **15**, 305–308.
Kim, S., Malinverni, J. C., Sliz, P., Silhavy, T. J., Harrison, S. C. & Kahne, D. (2007). *Science*, **317**, 961–964.
Knowles, T. J., Jeeves, M., Bobat, S., Dancea, F., McClelland, D., Palmer, T., Overduin, M. & Henderson, I. R. (2008). *Mol. Microbiol.* **68**, 1216–1227.
Knowles, T. J., Scott-Tucker, A., Overduin, M. & Henderson, I. R. (2009). *Nature Rev. Microbiol.* **7**, 206–214.
Laskowski, R. A., MacArthur, M. W., Moss, D. S. & Thornton, J. M. (1993). *J. Appl. Cryst.* **26**, 283–291.
Matthews, B. W. (1968). *J. Mol. Biol.* **33**, 491–497.
McCoy, A. J. (2007). *Acta Cryst.* D**63**, 32–41.
Mogensen, J. E. & Otzen, D. E. (2005). *Mol. Microbiol.* **57**, 326–346.
Otwinowski, Z. & Minor, W. (1997). *Methods Enzymol.* **276**, 307–326.
Perrakis, A., Morris, R. & Lamzin, V. S. (1999). *Nature Struct. Biol.* **6**, 458–463.
Schulz, G. E. (2003). *Adv. Protein Chem.* **63**, 47–70.
Sklar, J. G., Wu, T., Kahne, D. & Silhavy, T. J. (2007). *Genes Dev.* **21**, 2473–2484.
Thompson, J. D., Higgins, D. G. & Gibson, T. J. (1994). *Nucleic Acids Res*, **22**, 4673–4680.
Veenendaal, A. K., van der Does, C. & Driessen, A. J. (2004). *Biochim. Biophys. Acta*, **1694**, 81–95.
Voulhoux, R., Bos, M. P., Geurtsen, J., Mols, M. & Tommassen, J. (2003). *Science*, **299**, 262–265.
Vuong, P., Bennion, D., Mantei, J., Frost, D. & Misra, R. (2008). *J. Bacteriol.* **190**, 1507–1517.
Walther, D. M., Rapaport, D. & Tommassen, J. (2009). *Cell. Mol. Life Sci.* **66**, 2789–2804.
Wimley, W. C. (2003). *Curr. Opin. Struct. Biol.* **13**, 404–411.
Winn, M. D. *et al.* (2011). *Acta Cryst.* D**67**, 235–242.
Wu, T., Malinverni, J., Ruiz, N., Kim, S., Silhavy, T. J. & Kahne, D. (2005). *Cell*, **121**, 235–245.